

See discussions, stats, and author profiles for this publication at: <https://www.researchgate.net/publication/10764350>

# An Atomic Model for Actin Binding by the CH Domains and Spectrin-repeat Modules of Utrophin and Dystrophin

ARTICLE in JOURNAL OF MOLECULAR BIOLOGY · JUNE 2003

Impact Factor: 4.33 · DOI: 10.1016/S0022-2836(03)00422-4 · Source: PubMed

---

CITATIONS

57

READS

23

---

## 7 AUTHORS, INCLUDING:



Carolyn A Moores

Birkbeck, University of London

48 PUBLICATIONS 1,400 CITATIONS

[SEE PROFILE](#)



Roger Craig

University of Massachusetts Medical School

181 PUBLICATIONS 5,982 CITATIONS

[SEE PROFILE](#)



John Kendrick-Jones

University of Cambridge

189 PUBLICATIONS 10,825 CITATIONS

[SEE PROFILE](#)



William Lehman

Boston University

149 PUBLICATIONS 4,380 CITATIONS

[SEE PROFILE](#)



# An Atomic Model for Actin Binding by the CH Domains and Spectrin-repeat Modules of Utrophin and Dystrophin

**Andrew J. Sutherland-Smith<sup>1</sup>, Carolyn A. Moores<sup>1,2</sup>  
Fiona L.M. Norwood<sup>1</sup>, Victoria Hatch<sup>3</sup>, Roger Craig<sup>4</sup>  
John Kendrick-Jones<sup>1</sup> and William Lehman<sup>3\*</sup>**

<sup>1</sup>Structural Studies Division  
Medical Research Council  
Laboratory of Molecular  
Biology, Hills Road, Cambridge  
CB2 2QH, UK

<sup>2</sup>Department of Cell Biology  
Scripps Research Institute  
10550 N. Torrey Pines Road  
La Jolla, CA 92037, USA

<sup>3</sup>Department of Physiology and  
Biophysics, Boston University  
School of Medicine, 715 Albany  
Street, Boston, MA 02118  
USA

<sup>4</sup>Department of Cell Biology  
University of Massachusetts  
Medical School, 55 Lake  
Avenue North, Worcester  
MA 01655, USA

Utrophin and dystrophin link cytoskeletal F-actin filaments to the plasma-lemma. Genetic strategies to replace defective dystrophin with utrophin in individuals with muscular dystrophy requires full characterization of these proteins. Both contain homologous N-terminal actin-binding motifs composed of a pair of calponin-homology (CH) domains (CH1 and CH2) that are connected by spectrin-repeat modules to C-terminal membrane-binding sequences. Here, electron microscopy and 3D reconstruction of F-actin decorated with utrophin and dystrophin actin-binding constructs were performed using Utr261 (utrophin's CH domain pair), Utr416 (utrophin's CH domains and first spectrin-repeat) and Dys246 (dystrophin's CH domain pair). The lozenge-like utrophin CH domain densities localized to the upper surface of actin subdomain 1 and extended azimuthally over subdomain 2 toward subdomains 3 and 4. The cylinder-shaped spectrin-repeat was located at the end of the CH domain pair and was aligned longitudinally along the cleft between inner and outer actin domains, where tropomyosin is present when on thin filaments. The connection between the spectrin-repeat module and the CH domains defined the orientation of CH1 and CH2 on actin. Resolution of utrophin's CH domains and spectrin-repeats permitted docking of crystal structures into respective EM densities, leading to an atomic model where both CH and spectrin-domains bind actin. The CH domain–actin interaction for dystrophin was found to be more complex than for utrophin. Binding assays showed that Utr261 and Utr416 interacted with F-actin as monomers, whereas Dys246 appeared to associate as a dimer, consistent with a bilobed Dys246 structure observed on F-actin in electron microscope reconstructions. One of the lobes was similar in shape, position and orientation to the monomeric CH domains of Utr261, while the other lobe apparently represented a second set of CH domains in the dimeric Dys246. The extensive contact made by dystrophin on actin may be used *in vivo* to help muscles dissipate mechanical stress from the contractile apparatus to the extracellular matrix.

© 2003 Elsevier Science Ltd. All rights reserved

**Keywords:** actin; calponin homology domain; dystrophin; spectrin-repeat; utrophin

\*Corresponding author

Present addresses: A. J. Sutherland-Smith, Institute of Molecular BioSciences, Massey University, Private Bag 11222, Palmerston North, New Zealand; F. L. M. Norwood, Department of Neurology, Wessex Neurological Centre, Southampton General Hospital, Southampton SO9 4XY, UK.

Abbreviations used: ABD, actin-binding domain; ABS, actin-binding sequence; CH, calponin-homology; CH1, and CH2, the two respective calponin-homology domains comprising an ABD; Dys246, dystrophin amino acid residues 1–246; EM, electron microscopy; Utr261, and Utr416, utrophin amino acid residues 1–261 and 2–416, respectively.

E-mail address of the corresponding author:  
wlehman@bu.edu

## Introduction

Dystrophin, a large multi-domain protein (427 kDa), binds the dystroglycan complex of the muscle plasma membrane and links the actin cytoskeleton to the extracellular matrix. Duchenne and Becker muscular dystrophies are caused by mutations or the deletion of dystrophin, leading to fragility in muscle and associated increased levels of intracellular  $\text{Ca}^{2+}$ , proteolytic activity and myofibrillar decomposition.<sup>1–3</sup> Utrophin (395 kDa), the autosomal homologue of X-linked dystrophin, is distributed more widely than dystrophin, being found in developing muscle, brain, kidney, liver, spleen, stomach, neuronal and vascular tissues.<sup>1–3</sup> Utrophin is present in differentiated muscle cells, but is restricted to the neuromuscular and myotendinous junctions. Sequence analysis reveals that dystrophin and utrophin molecules can be divided into three functionally distinct regions.<sup>4</sup> They both contain an N-terminal actin-binding domain (ABD) consisting of two CH domains, an elongated central region consisting of multiple three-helix bundles (24 for dystrophin, 22 in utrophin) homologous to those found in spectrin, and a C-terminal region containing a WW domain, EF hands, a cysteine-rich domain and a coiled-coiled region. The C-terminal regions interact with the membrane glycoprotein complex composed of the  $\alpha$  and  $\beta$  dystroglycans, the sarcoglycan complex ( $\alpha$ ,  $\beta$ ,  $\gamma$  and  $\delta$ ) and sarcospan, a series of integral and peripheral membrane proteins that bridge the sarcolemma to the extracellular matrix. In addition, the C-terminal domains interact with the adaptor proteins dystrobrevin and syntrophin, which are themselves associated with nitric oxide synthase, ErbB4 receptor protein kinase and voltage-gated sodium channels in the plasma membrane.<sup>1–3</sup> Dystrophin is vital for stabilizing this elaborate plasma membrane assembly.<sup>5</sup> In addition, by forming part of a bridge from the actin cytoskeleton to the extracellular matrix, dystrophin is thought to act as a cellular shock-absorber, limiting damage to the sarcolemma during contraction and extension of muscle fibers.<sup>1,2</sup> Utrophin presumably performs related functions at neuromuscular and myotendinous junctions and in non-muscle tissues.

Dystrophin and utrophin are members of the spectrin-like family of actin-binding proteins, which includes the oligomeric actin crosslinking proteins spectrin and  $\alpha$ -actinin.<sup>6</sup> All members of the family contain homologous N-terminal ABDs and multiple three-helix “spectrin” repeat regions. CH1 and CH2, the two “sub-domains” of the ABDs, each share sequence similarity with the so-called calponin homology (CH) domain of the smooth muscle protein calponin.<sup>7</sup> Further sequence comparisons have revealed a greater degree of similarity between CH1 (or CH2) domains among different members of the family than between the CH1 and CH2 domains from the same protein.<sup>8</sup> ABDs are found in proteins lacking spectrin-repeats, although the manner in which they are

employed differs, depending on the other regions present in the protein. For example, the fimbrin molecule contains two tandem ABDs (i.e. two sets of CH1CH2 modules) involved in actin filament bundling.<sup>9</sup> Single CH-domain-containing proteins are present in smooth muscle calponin and SM22/transgelin, and in certain signaling proteins such as Vav and IQGAP.<sup>7,10</sup> However, binding studies have indicated that the single CH-domain is not sufficient for actin binding.<sup>10</sup>

Binding assays using protein fragments,<sup>11–15</sup> peptide NMR<sup>16</sup> and antibody protection studies<sup>17</sup> have identified three consensus sequences within the ABDs of utrophin, dystrophin and related proteins that are believed to be important for actin binding. Actin binding sequences (ABS) 1 and 3 are located near the N terminus of the CH1 and CH2 domains, respectively, while ABS sequence 2 maps to a different region of CH1. These results as a whole indicate that both CH1 and CH2 contribute to actin binding and presumably bind to actin as a unit.

Crystal structures of dystrophin (PDB entry 1dxx),<sup>18</sup> utrophin (PDB entry 1qag),<sup>19</sup> and fimbrin (PDB entry 1aoa)<sup>20</sup> ABDs reveal that the structures of the individual CH1 and CH2 domains are very similar and are composed of a simple globular scaffold of four major helices. The three crystal structures reveal that the actin-binding sequences (ABS) regions 1, 2 and 3 identified as being important for actin binding do not form a continuous surface, again suggesting that CH1 and CH2 domains are both necessary for actin binding. However, the manner in which CH1 and CH2 are organized within these crystal structures is strikingly different. The fimbrin ABD crystallizes as a monomer with a compact globular structure resulting from the close apposition of CH1 and CH2 about a connecting  $\alpha$ -helical hinge. In contrast, dystrophin and utrophin form anti-parallel dimers of two ABDs, in which each component monomer adopts an extended dumbbell conformation, with CH1 and CH2 separated by an opening of the central  $\alpha$ -helical hinge. Within the dystrophin and utrophin dimers, however, domain-swapping of CH-domains between monomer chains A and B results in a CH1–CH2 interface virtually identical with that of the fimbrin ABD. Thus CH1 and CH2 from opposing monomer partners align to form new domain pairs with new binding interfaces (CH1A–CH2B and CH1B–CH2A), each comparable in structure to that of the monomeric fimbrin ABD.<sup>18–20</sup> Whether such ABD dimerization occurs *in vivo* or is an artifact of crystallization has not been established, since, in solution, the utrophin ABD is clearly monomeric,<sup>21</sup> whereas, in contrast, the dystrophin ABD exists in a monomer-dimer equilibrium.<sup>22</sup> No high-resolution structure for an ABD–spectrin complex has been solved, but crystal structures of various spectrin-repeat modules from spectrin itself and from  $\alpha$ -actinin have all revealed a three-helix bundle, barrel-like structure with the major differences lying in the loops

connecting the helices. These three-helix bundles form the rod elements in their parent cytoskeletal proteins and have been shown to bind to other cytoskeletal and signaling molecules.<sup>23</sup>

Considerable interest in utrophin has been stimulated by the possibility of over-expressing the protein in patients afflicted with muscular dystrophy and thereby replacing the deficient or defective dystrophin with a functional homologue. Studies showing that an utrophin transgene alleviates the disease symptoms in the *mdx* mouse model of muscular dystrophy<sup>24,25</sup> have provided encouragement for this approach. Understanding the potential value of therapeutic replacement of dystrophin with utrophin requires the complete structural and functional characterization of these two proteins, including the molecular nature of the interaction of the actin cytoskeleton with dystrophin and with utrophin. Previous structural studies have examined the binding of isolated ABDs to actin.<sup>26,27</sup> Here, we have extended these studies, by probing for a role of multi-domain contacts in actin binding. On the basis of electron microscopy (EM) studies and 3D helical reconstruction, we present structural information on the binding of the utrophin ABD in combination with the first of its three-helix repeat regions. We tested whether the ABD bound to actin in a compact form similar to fimbrin<sup>20,28,29</sup> or as extended structures<sup>26,27</sup> like those seen in utrophin and dystrophin crystals.<sup>18,19</sup> Our studies have enabled us to propose a likely molecular model for the binding of utrophin CH domains and spectrin-modules on actin. For comparison, the dystrophin ABD was studied to determine whether the dystrophin and utrophin ABDs have similar or distinct modes of actin association.

## Results

### Electron microscopy of F-actin decorated with utrophin and dystrophin constructs

#### Labeling with CH-domains

To determine the organization and shape of N-terminal CH domains of utrophin and dystrophin on actin, F-actin was complexed with engineered CH domain constructs of utrophin (Utr261) and dystrophin (Dys246), under conditions that should saturate filaments with these proteins (see Materials and Methods). Electron micrographs of negatively stained F-actin–Utr261 and F-actin–Dys246 consistently showed uniform decoration of F-actin. Binding of the ABD constructs was evident from the increase in diameters of the Utr261 and Dys246-decorated filaments, which were about 1.5 and 1.65 times as wide as unlabeled F-actin, respectively (**Figure 1(a), (b) and (e)**). The uniformity in labeling suggested full decoration. Visualization of actin substructure was partially masked by the decoration, although the

36 nm crossover repeat of the actin filaments was very obvious.

Electron micrographs of unstained frozen-hydrated F-actin–Utr261 filaments were evaluated to assess any possible effects of stain fixation and filament drying.<sup>26</sup> Cryo-EM again showed uniformly decorated filaments and no evidence of heterogeneous labeling (**Figure 1(c)**). Cryo-EM was attempted on F-actin–Dys246, but this was not pursued, since Dys246 did not label F-actin effectively under cryo-EM conditions, presumably because of the low affinity of the Dys246 for F-actin ( $K_d$  10–40  $\mu\text{M}$ ).

#### Labeling with CH domains and spectrin modules

To assess the interactions of actin and multi-domain constructs more closely approximating native utrophin, F-actin was labeled with Utr416, which contains the first spectrin-repeat module of utrophin connected to the utrophin N-terminal CH domains. Attempts at saturating F-actin completely with this construct led to filament aggregation and massive background interference by unbound protein. However, EM images of F-actin labeled with a moderate excess of Utr416 showed a mixture of variably decorated and undecorated filaments with less background interference and little filament aggregation (**Figure 1(d)**). Those filaments with the highest degree of decoration were chosen for further analysis. The microscopy on Utr416-decorated filaments was superior to that performed on filaments labeled with UT11, a 592 amino acid residue N-terminal utrophin construct with CH domains and two spectrin repeats,<sup>30</sup> and structural studies on UT11 were not pursued.

#### The 3D reconstructions of reconstituted thin filaments

Even though each set of filaments investigated was obviously decorated, the locations, orientations and shapes of the constructs could not be discerned directly from any of the EM images recorded, and molecular details of different structures could not be compared to each other. To determine the organization of the CH domains on F-actin, image processing and 3D reconstruction was therefore necessary. This was relatively straightforward, since the labeled filaments were quite straight and were not aggregated.

Density maps of labeled filaments were calculated by inverse Fourier transformation of the averages of Fourier transform layer-line data (not shown). These maps all showed clear filament polarity and typical two-domain actin subunits that could be further divided into subdomains (**Figures 2 and 3**). When compared with maps generated from pure F-actin controls, all reconstructions displayed obvious extra density, described below, that had high statistical significance (>99.9% confidence levels).

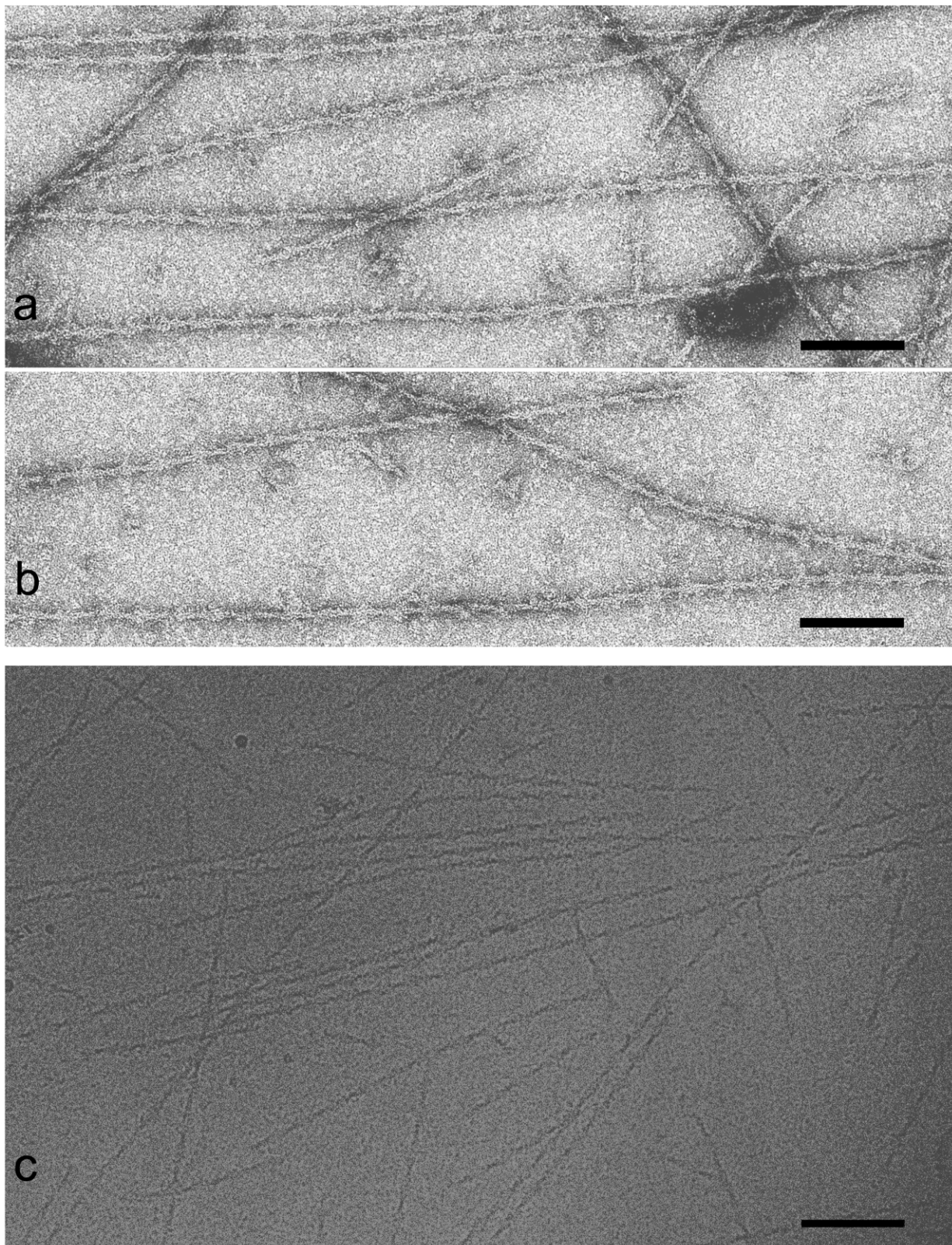


**Figure 1** (legend opposite)

#### *F-actin–Utr261 filaments*

Reconstructions of negatively stained and frozen-hydrated F-actin–Utr261 both exhibited a

lozenge-shaped extra density that labeled each actin monomer along the filaments as a discrete mass measuring approximately  $30 \text{ \AA} \times 30 \text{ \AA} \times 55\text{--}60 \text{ \AA}$  ([Figures 2 and 3](#)). These dimensions were

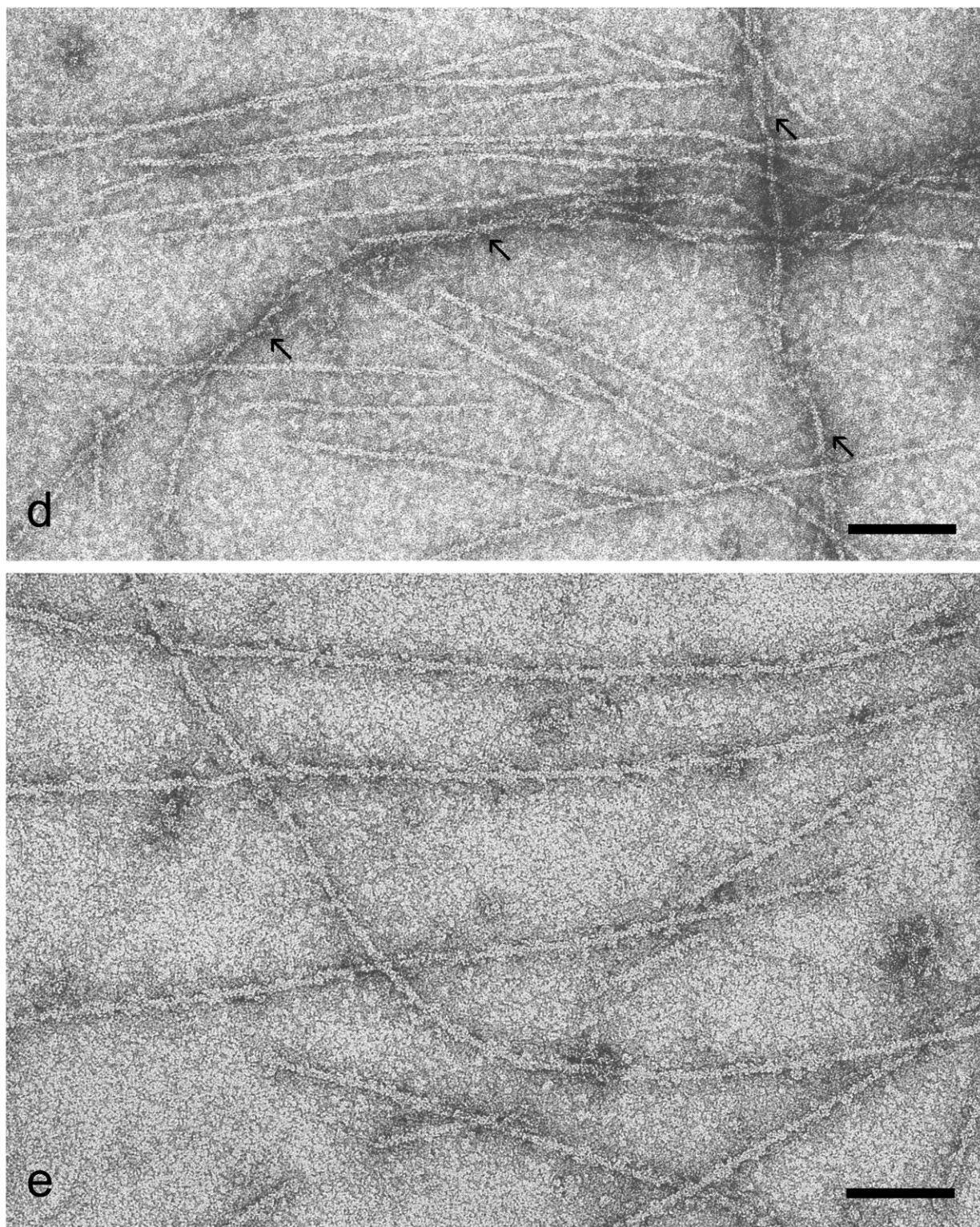


**Figure 1.** Electron micrographs of decorated thin filaments. (a)–(c) F-actin–Utr261; (d) F-actin–Utr416; (e) F-actin–Dys246. (a) and (b) Negative staining and (c) cryo-EM of F-actin saturated with Utr261 showed well dispersed, homogeneously labeled filaments. (d) Negative staining of F-actin–Utr416 provided areas where filaments were well decorated and generally dispersed with only small amounts filament aggregation evident (aggregated groups of filaments indicated by arrows). (e) Negatively stained F-actin–Dys246 filaments were decorated completely and had diameters slightly wider than those of F-actin–Utr261; these filaments were well dispersed and showed no evidence of filament crosslinking. Mixtures of F-actin and Dys246, examined by cryo-EM, gave little indication of decoration (not shown). Individual filaments are best viewed at an oblique angle along their long axis. The scale bar represents 100 nm.

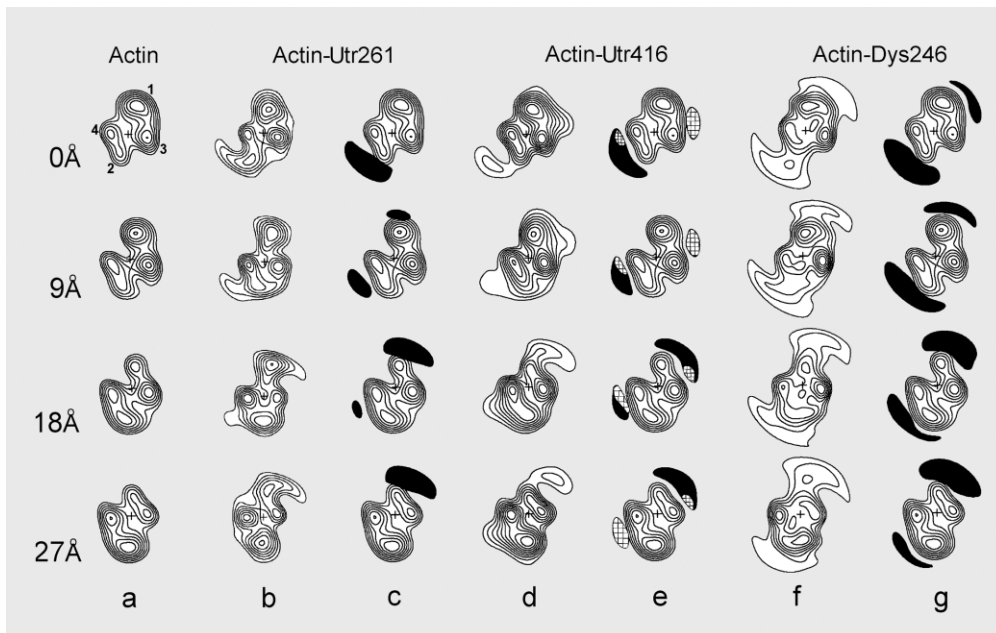


**Figure 2.** Transverse sections (*z*-sections) through 3D reconstructions of negatively stained filaments. The relative positions of actin-bound constructs over a span of 27 Å (approximately one-half the axial dimensions of the actin monomer) are shown. Because actin monomers are staggered by approximately  $0.5 \times 55$  Å in one helical strand with respect to the other, sectioning through subdomains 1 and 3 of one actin monomer (subdomains numbered in the F-actin member of the 0 Å series) results in sectioning through subdomains 2 and 4 of the adjacent monomer. (a) F-actin control; (b) and (c) F-actin–Utr261; (d) and (e) F-actin–Utr416; (f) and (g) F-actin–Dys246. The maps characterizing decorated filaments are shown in pairs, those on the left ((b), (d) and (f)) represent sections through reconstructions of the decorated filaments, those on the right ((c), (e) and (g)) show corresponding difference densities, attributable to each bound construct (calculated by subtracting F-actin from respective decorated maps), superimposed on F-actin. Difference density contributions from CH domains (filled black in (c), (e) and (g)) and from spectrin-repeats in (e) (cross-hatched, determined by subtracting the maps of F-actin–Utr261 from F-actin–Utr416) are highlighted. Sections shown are at the same axial position along F-actin of the reconstructions and have the same relative orientation. All densities shown are significant at confidence levels greater than 99.9%. Note that most of the CH domain density contribution lies adjacent to actin subdomain 2 and projects azimuthally towards subdomain 4. In contrast, the spectrin-repeat density localizes over the junction between subdomains 1 and 3, and subdomains 2 and 4. The reconstructions shown were derived from 24 F-actin–Utr261, 23 F-actin–Utr416 and 32 F-actin–Dys246 filaments. The average phase residuals ( $\Psi \pm SD$ ), a measure of the agreement among filaments generating reconstructions for the averaged data sets were  $58.8(\pm 6.0)^\circ$ ,  $64.6(\pm 5.2)^\circ$ ,  $67.5(\pm 4.3)^\circ$ , respectively. The corresponding average up–down phase residuals ( $\Delta\Psi \pm SD$ ), a measure of filament polarity were  $13.3(\pm 7.1)^\circ$ ,  $16.5(\pm 5.2)^\circ$ ,  $12.1(\pm 4.8)^\circ$ . The resolution of the maps was between 25 Å and 32 Å.

similar to those of the crystal structure of Utr261 modeled as a compact monomer, i.e. where the two-component CH domains of Utr261 are in a tightly packed, closed configuration like fimbrin.<sup>20</sup> Utr261 localized to the upper surface of actin subdomain 1 and projected over subdomain 2 azimuthally to subdomains 3 and 4 (Figure 3). There was no suggestion of additional mass connecting Utr261 densities on adjacent actin monomers or obvious indications of Utr261 assuming an extended configuration. The shape and orientation of the extra density was evident in the maps of all filaments averaged. The extra mass attributable to the Utr261 construct became especially apparent when difference densities computed between maps of F-actin–Utr261 and F-actin were superimposed on the atomic model F-actin that, in turn, had been fitted to our maps (Figure 5). No obvious difference was apparent between reconstructions generated from filaments

that were negatively stained or preserved in ice (Figure 4). However, the resolution obtained for negative staining (~25 Å) was greater than for cryo-EM (~35 Å), and therefore the definition of the edges of the Utr261 was better in maps of stained filaments.

#### F-actin–Dys246 filaments

Binding studies indicate that Utr261 interacts with thin filament actin as a 1:1 (Utr261 to actin monomer) complex,<sup>21</sup> whereas the CH domains of dystrophin (Dys246) bind as a 2:1 complex (see Materials and Methods). Therefore, it was of great interest to determine the corresponding structural differences in the association of the two constructs with actin. Reconstructions of F-actin–Dys246, like those of F-actin–Utr261, showed density on the upper surface of actin subdomain 1 that projected over subdomain 2 azimuthally to subdomains 3

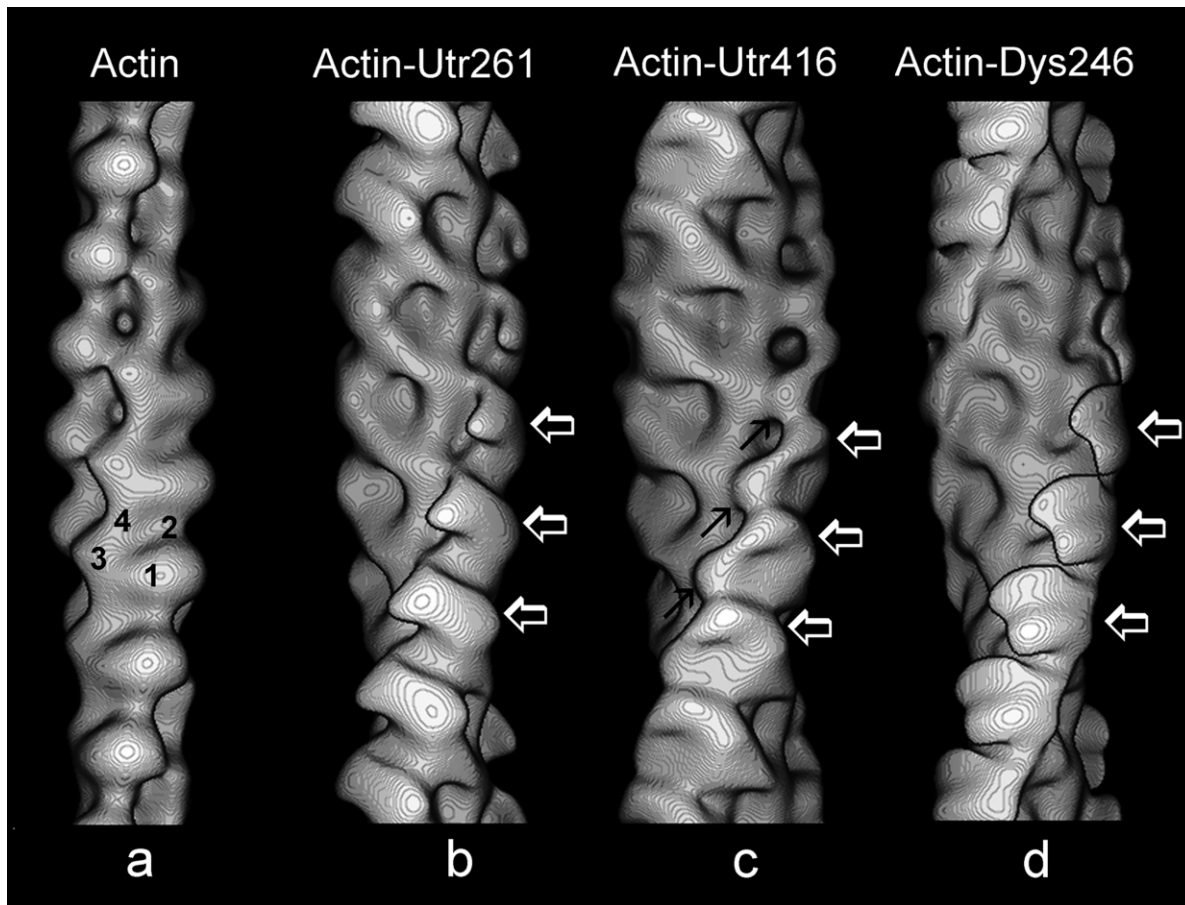


**Figure 3.** Surface views of thin filament reconstructions showing the positions of CH-domains and spectrin-repeats. (a) F-actin control (actin subdomains numbered on one monomer); (b) F-actin–Utr261; (c) F-actin–Utr416; (d) F-actin–Dys246. The reconstructions are shown with the pointed end of the filaments facing up; they were aligned so that densities in the F-actin backbone of each have the same axial and rotational orientation. Note the contribution from CH domains indicated by horizontal white-outlined arrows in (b), (c), and (d), and from spectrin-repeat modules in (c) denoted by oblique black arrows. The utrophin CH domains (b) in F-actin–Utr261 form lozenge shaped densities attached to successive actin monomers on the upper surfaces of subdomain-1 and project at a slightly oblique angle ( $\sim 20^\circ$ ) over subdomain-2 towards the inner domain of actin whereas, (c) in F-actin–Utr416 CH domains are slightly more horizontal and are attached to spectrin densities, not seen in F-actin–Utr261. The spectrin density itself shows connectivity to the tip of the CH domain and is oriented axially along the cleft formed between inner and outer actin domains. (d) CH domains in Dys246 differ from those derived from utrophin and are characterized by bilobed azimuthally oriented densities, presumably representing two ABDs bound to each actin monomer.

and 4 (Figure 3). However, Dys246 differed from the Utr261 density, by forming a bilobed mass that was attached to each actin monomer. The size of the bilobed density was approximately double that of unilobed Utr261. One of the lobes of Dys246 was similar in shape and orientation to Utr261, and the second lay parallel with the first at slightly higher radius. The contribution of bilobed Dys246 to the overall filament reconstruction became very apparent when superimposed as a difference density on the atomic structure of F-actin (Figure 5).

#### F-actin–Utr416 filaments

Reconstructions of F-actin, decorated with Utr416, i.e. with utrophin's first spectrin-repeat and its CH domains, were generated for comparison and to determine the potential binding contri-

butions of the constituent spectrin module. The reconstructions revealed densities attributable to both CH domain and spectrin regions of the Utr416 construct labeling filaments on each actin monomer (Figures 2 and 3). Part of the mass tagging actin no doubt represented the CH domain contribution, since its shape and azimuthal orientation was comparable to that of the Utr261. This density contribution was slightly smaller than that of Utr261, presumably because the filaments analyzed were decorated variably, and hence stretches of partially and fully decorated actin may have been averaged together. In addition, densities were noted that had been not seen in the reconstruction of F-actin decorated with the Utr261 construct. These extra densities, apparently contributed by the spectrin-repeat, were observed at the junction of actin subdomains 1 and 3 (indicated by a diagonal arrow in Figure 3) and were

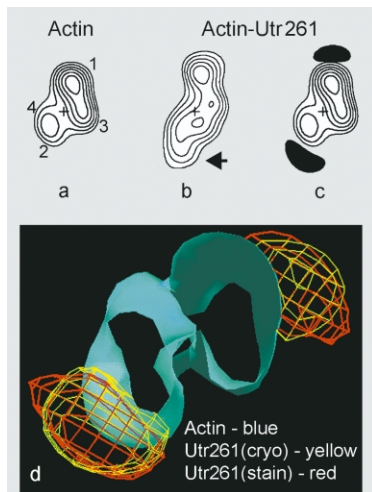


**Figure 4.** Reconstructions of cryo-EM filaments. (a), (b) Transverse sections through reconstructions of frozen-hydrated F-actin and F-actin–Utr261. (a) F-actin control (subdomains numbered); (b) F-actin–Utr261; (c) Utr261 difference densities (filled black) obtained by subtracting the maps of F-actin in (a) from those of F-actin–Utr261 in (b), then superimposed on F-actin. The three sections shown are at the same axial position along F-actin and have the same relative orientation. In (b), the map of F-actin–Utr261, note the large extra density contributed by the utrophin CH domains (marked by an arrow) that is found over actin subdomain 2 and is not present in the F-actin control. The CH domain contribution is evident in (c), where difference density analysis shows a tangential attachment of the mass on subdomain 1 of actin and azimuthal extension over subdomain 2. The reconstruction of frozen-hydrated F-actin–Utr261 was generated from 28 filament images; the average phase residual among filaments generating the average was  $56.1(\pm 5.5)^\circ$  and the corresponding average up-down phase residual ( $\Psi \pm SD$ ) was  $20.6(\pm 5.4)^\circ$  (these values compared very favorably to those obtained by Moores *et al.*<sup>26</sup>). Densities in the maps are significant at confidence levels greater than 99.9%. The resolution for the F-actin–Utr261 reconstruction was about 35 Å. (d) Comparison of Utr261 bound to F-actin visualized by negative staining and by cryo-EM of F-actin–Utr261. To more easily judge if the Utr261 binding to F-actin was the same in reconstructions of F-actin–Utr261 derived from negatively stained and frozen-hydrated samples, Utr261 positions on actin were determined as above by difference analysis and their respective densities superimposed on a common ~30 Å thick transverse slab of F-actin (actin, blue; cryo-Utr261 densities, yellow; negative stain densities, red). The comparison shows that utrophin ABD decoration of F-actin is virtually the same by both methods of filament preservation. Analogous images of the two densities displayed on longitudinally oriented F-actin lead to the same conclusion (not shown).

connected to the tips of the CH domains by a thin stalk, giving the impression that the CH domain was pulled towards the spectrin density. The only connectivity detected between Utr416 densities on adjacent actin monomers was *via* the spectrin domain; CH domain regions on successive actin monomers were not connected directly. These

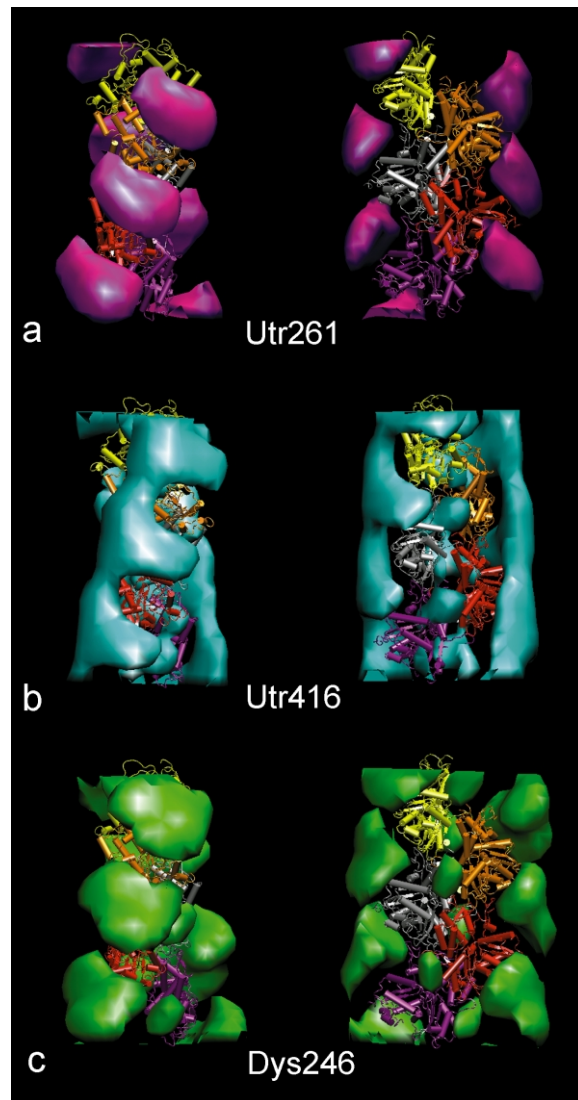


**Figure 5.** Depiction of ABDs as difference densities on the atomic model of F-actin. Difference densities representing actin bound proteins were generated by subtracting maps of F-actin controls from maps of decorated F-actin; (a) Utr261 (magenta), (b) Utr416 (cyan) and (c) Dys246 (green) densities are represented as solid volumes. Two orthogonal views are shown for each map. The densities are shown superimposed onto the atomic model of F-actin<sup>54</sup> (in cartoon representation) that had been fitted to the actin portion of the reconstructions. The F-actin filaments (here and in Figures 6–8) are oriented with their pointed end up. The difference maps have been contoured at  $2.4\sigma$  above the mean. This Figure (and Figures 6–8) was prepared with VMD.<sup>63</sup>

observations were corroborated by difference density analysis comparing F-actin–Utr416 with F-actin (Figure 5).

### Molecular fitting of CH domains and spectrin modules to 3D reconstructions

#### Utrophin 261 and utrophin 416 docking

Despite the generally conserved nature of CH

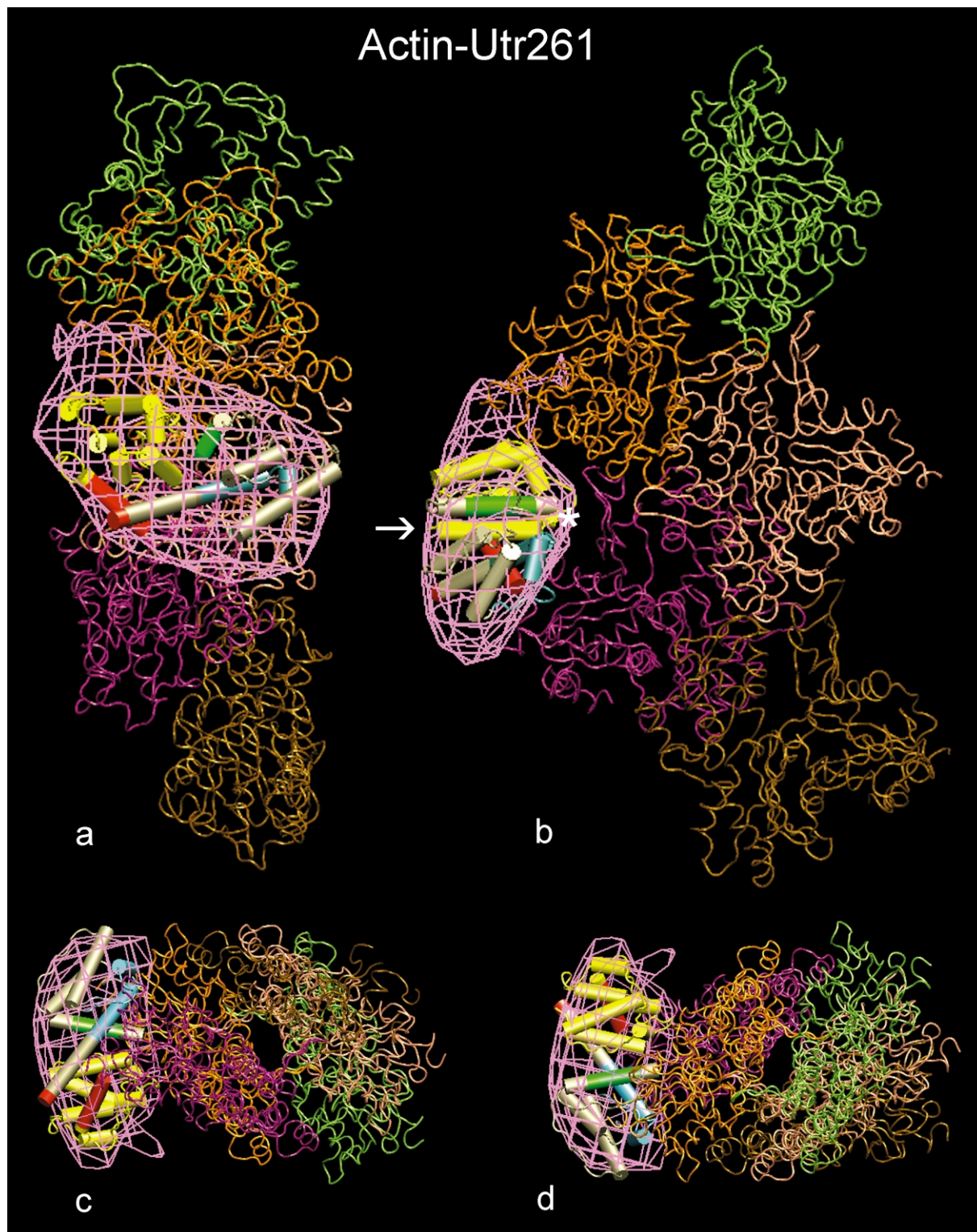


**Figure 6.** Docking of Utr261. The atomic model of the Utr261 construct was docked as a compact monomeric structure into its corresponding EM density envelope (pink wire-cages) determined by difference density analysis as above. Note the goodness of fit. The density envelopes are again shown superimposed on the atomic model of F-actin. Only one ABD is shown bound to a five-monomer long stretch of the F-actin atomic model to simplify the display. The orientation of the atomic model shown corresponds to SITUS solution 3 for Utr261 (the only high-scoring solution that places the CH2 subdomain close to the spectrin-repeat density observed in the Utr416 reconstruction; see [Figure 7](#) and the description in the text). The actin is shown as an  $\alpha$ -carbon tube and the Utr261 as a molecular cartoon. The CH1 subdomain is colored silver-gray and CH2 yellow. The ABS sites are color-coded: ABS1, green (residues 34–43); ABS2, cyan (residues 105–132), ABS3, red (residues 147–163); the C terminus of the ABD is indicated by an arrow and the N terminus by an asterisk (\*) in (b). Four orthogonal views are shown: (a) and (b) longitudinal views with the pointed end of F-actin facing up; (c) and (d) transverse views observed from the barbed to the pointed end of F-actin in (c), and from the pointed end to the barbed end in (d). The difference maps have been contoured at  $2.4\sigma$  above the mean.

**Table 1.** SITUS fitting results

Utrophin ABD		Dystrophin ABD		Spectrin-repeat	
Solution number	Correlation coefficient	Solution number	Correlation coefficient	Solution number	Correlation coefficient
1	0.5785	1	0.4054	1	0.1603
2	0.5783	2	0.4031	2	0.1603
3	0.5544	3	0.4013	3	0.1603
4	0.5544	4	0.4008	4	0.1598
5	0.5469			5	0.1575
6	0.5008			6	0.1574
				7	0.1542
				8	0.1506
				9	0.1478
				10	0.1458

SITUS<sup>56,57</sup> refines the ten best fits and then degenerate solutions are removed automatically. For the fitting of Utr261, no clear discrimination between the highest-value solutions was evident from correlation coefficient comparison or from visual examination. Solutions 1 and 2 determined by SITUS differed only slightly from each other and were considered equivalent. Solutions 3 and 4 were an equivalent pair and related to 1 and 2 by a 2-fold rotation of the model about an axis parallel with the long filament axis. Both these pairs of solutions fitted the EM density well (Figure 6). Solution 5 placed the model partially outside the density, even though its correlation coefficient was similar to those of solutions 1–4. Solution 6 was even poorer and the latter two solutions were not considered further. For Dys246, solution 1 was equivalent to solutions 1 and 2 for the Utr261 fitting, and the second solution to Utr261 solution 3.

domain pairs, these ABDs have been reported to interact with actin as compact<sup>20,28,29</sup> or extended structures.<sup>26,27</sup> In principle, molecular docking of crystal structures to corresponding EM densities should resolve this ambiguity. The dimensions and shape of the density attributable to Utr261 in our reconstructions (Figures 4–6) indicated that the ABD was compact and not elongated. Visual inspection of the highest-scoring solutions calculated by the automated fitting program SITUS (designed to fit crystal structures to EM maps, see Materials and Methods) revealed that the position of the utrophin CH domain pair, modeled as a compact monomer, could be clearly defined. The best solutions (Table 1) placed the crystal structure of the ABD nicely within the corresponding EM density with only minimal parts of the atomic model lying outside of the envelope (Figure 6). However, different solutions determined by the program oriented the compact crystal structure model equally well, but in completely different directions. Unlike very asymmetrical proteins such as actin and S-1, CH domains themselves and CH domain pairs are nearly ellipsoidal and thus more symmetrical in shape, making molecular docking of even the best of computationally fitted maps difficult to evaluate. Without further information, the hybrid crystallography procedure was not definitive. The SITUS routine did help limit the search for the best fitting to a few choices and, as described below, only one of these solutions made sense in the context of other results.

The close apposition of CH1 and CH2 in the compact model of Utr261 results in a symmetrical structure at low resolution and, for reasons just outlined, an indeterminate position of the two sub-domains in Utr261 density envelopes. However, an asymmetry was introduced in Utr416 by the presence of the spectrin-repeat, in effect marking the C-terminal end of the utrophin ABD CH2-sub-domain. In Utr416, the known connectivity

between the CH2 subdomain and the spectrin-repeat now imposed constraints on the ABD modeling, since the CH2 must be in close proximity to the spectrin-repeat for the two to be joined together. This could be satisfied only by CH2 facing the inner domain of actin and nearly abutting the spectrin-repeat, with CH1 therefore oriented towards the outer domain, an orientation represented by SITUS solution 3 for Utr261 (Table 1). Hence, the alignment of the ABD within Utr416 could be determined by its position relative to the spectrin module.

In this model, the C terminus of CH2 is located on the surface of the filament close to the spectrin-module. Alternatively, when CH domains were rotated ~180° about an axis parallel with the actin filament (the other potential alignment according to SITUS, see notes to Table 1), the shortest path between the spectrin module and the C terminus of CH2 would be implausibly long. Even ignoring this consideration, the C-terminal end of CH2 in the latter arrangement would be buried between the CH domain and actin, an unlikely origin for a peptide linked distally to spectrin.

The spectrin-repeat density in Utr416 maps was delineated after positioning the ABD. A precise fitting of the spectrin-repeat itself was difficult, because its shape also lacked asymmetric features. The EM density for this region of Utr416 was essentially cylindrical and, at low resolution, the corresponding three-helix spectrin-repeat structure had a similar profile when rotated radially or by 180° about its longitudinal axis. Even, the SITUS routine, using a spectrin-repeat search template, failed to convincingly find a suitable orientation (correlation coefficients <0.2, Table 1), but did provide a valuable set of models that could be drawn on for visual analysis. Solution 6 was chosen as the most appropriate model for the spectrin position as this placed the N terminus of the spectrin-repeat at a reasonable distance from the CH2

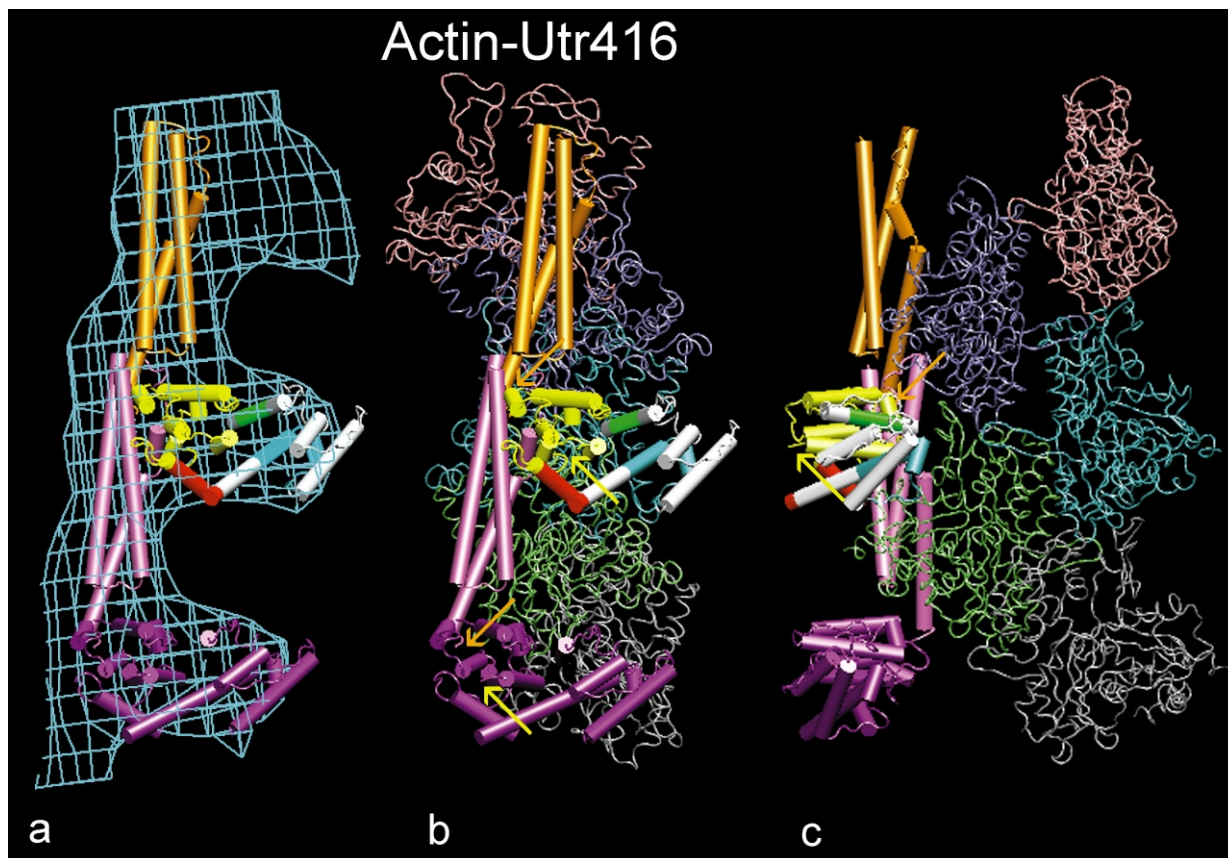


**Figure 7.** Docking of Utr416. (a) The atomic models of the ABD structure and spectrin-repeat module shown docked separately into the EM density envelope of Utr416 (cyan wire-cage) determined by difference density analysis as described for [Figure 5](#). The model for the ABD orientation again represents SITUS solution 3 that places CH2 close to the spectrin-repeat density in the reconstruction. The docking of two ABDs is shown; in the upper ABD, CH1 is colored white and CH2 yellow, the entire lower ABD is shown in dark magenta; two adjacent spectrin-repeats are displayed in gold and light-magenta (the spectrin-repeat positions represent solution 6; see [Table 1](#), column 3). The ABS sites are color-coded as above. The difference maps were contoured at  $2.0\sigma$  above the mean, and the difference density (and Utr416 model) from the far side of the filament has been removed for clarity. (b) and (c) Two orthogonal views of Utr416, modeled as in (a), shown bound to F-actin; Utr416 again shown on only one side of the filament for simplicity; orientations in (a) and (b) are the same. The actin is represented as an  $\alpha$ -carbon tube and the Utr416 as a molecular cartoon. The domains are colored and sequences are highlighted as described for [Figure 6](#). Positions for the C terminus for CH2 and the N terminus for the spectrin-repeats are in (b) and (c) indicated by yellow and orange arrows, respectively.

C terminus, a distance that could be spanned by the 46 amino acid residues that link the two domains together. Based on its sequence, the linker region is predicted to contain two or three  $\alpha$ -helices sufficiently long to span the requisite 27 Å separation. All other solutions placed the spectrin-repeat too far away from the CH2 domain to be connected by the linker. The connectivity of the spectrin-repeat to the ABD was confirmed by contouring the Utr416 difference density map at increasingly higher contour levels until a break in the density occurred. This suggested that the connection of the spectrin-repeat (and therefore its N terminus) faced the barbed end of the filament, with the rest of the repeat directed towards the pointed end. This orientation was consistent with only the alignment arrived at in solution 6 for the spectrin-repeat ([Table 1](#); [Figure 7](#)). Minimal overlap was observed between ABDs and spectrin-repeats fitted on successive monomers of F-actin according

to solutions 3 and 6 ([Figure 7\(b\)](#)). No information is available to orient the spectrin-repeat around its cylindrical axis, and this remained ambiguous.

The molecular model described above indicates that the CH1 subdomain lies on top of and across a broad surface of subdomain 1 of each actin monomer, whereas CH2 lies closer to the inner region of the filament ending near subdomain 1 of the next actin monomer along the long-pitch actin helix (in the direction of the filament pointed end). Accordingly, regions of the utrophin ABD forming the binding surface with actin appear to include the N terminus (close to ABS1) and other parts of the CH1 subdomain (residues 54–62, 103–110 and 120–133) that partially overlap with ABS2. Regions of CH2 that are in close proximity to F-actin include residues 154–156 (part of ABS3), 173–182 and 228–240. Thus the organization of the ABD determined here is consistent with the available biochemical data on actin-binding sites, even

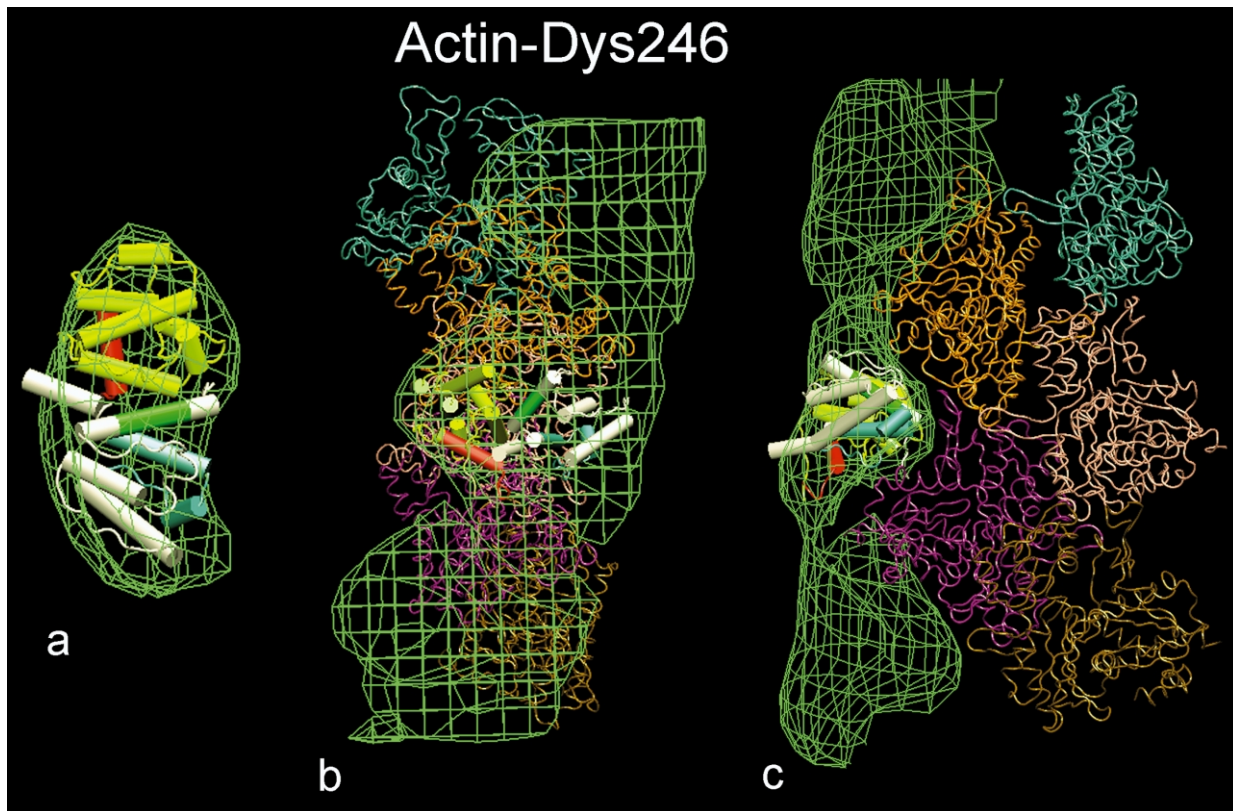


**Figure 8.** Docking of Dys246. The atomic model of the Dys246 construct was docked as a compact monomeric structure into its corresponding EM density envelope (green wire-cage) determined by difference density analysis as above. The atomic model shown represents SITUS solution 2 for Dys246. (a) A transverse view of EM densities and the docked Dys246 monomer structure. Note that Dys246 fit very well into the major aspect of the EM envelope. Comparison with Utr261 in Figure 6(d) shows that the SITUS alignment of the two ABDs was virtually the same. (b) and (c) Longitudinal views of the EM densities and the Dys246 monomer structure shown superimposed on F-actin. The monomer model of Dys246 did not fill the entire EM envelope; what remained, however, was not large enough to accommodate a second Dys246 monomer. The actin is represented as an  $\alpha$ -carbon tube and the Dys246 as a molecular cartoon. The CH1 domain is colored white and the CH2 domain in yellow. The ABS sites are color-coded: ABS1, green (residues 18–27); ABS2, cyan (residues 88–116); ABS3, red (residues 131–147). The difference maps have been contoured at  $2.4\sigma$  above the mean.

though the latter information was not a factor in the modeling. Interestingly, the spectrin-repeat domain lies over subdomains 3 and 4 in a similar location and orientation as that adopted by the tropomyosin coiled-coil when it is bound to F-actin.<sup>31</sup>

#### Dystrophin 246 docking

Attempts were made to dock atomic models of the CH domains of dystrophin to the bilobed EM density envelope of Dys246. Dystrophin modeled as a compact monomeric ABD model fitted into the inner lobe of density after applying the coordinates determined by solution 3 for Utr261 (the fitting of choice as described above). Moreover, SITUS fitting with Dys246, organized as a monomeric structure, docked the structure into the same location in the inner density lobe. Here, the top solution was equivalent to solutions 1 and 2 for the Utr261 fitting, and the second solution to Utr261 solution 3 (Table 1). Thus, SITUS docked

the dystrophin and utrophin ABDs into comparable positions in their respective difference maps, even though, as pointed out above, a single dystrophin ABD does not account for all the difference density detected in the Dys246-labeled filaments (Figure 8). However, it was not possible to successfully fit the dimeric structure into the entire density envelope using SITUS, as the outer density lobe was not large enough to accommodate any ABD model when it was contoured at acceptable levels. This could be explained if our decorated filaments bound mixtures of dimers and compact monomers, which would have the weakened dimer contribution and compromised attempts to dock a dimeric crystal structure. Alternatively, if only one ABD partner of a dimer bound tightly enough to actin to provide a strong signal, this would have had the same effect.

#### Discussion

Our goal is to fully understand the structural

contributions of both utrophin and dystrophin to the cortical cytoskeleton of muscle cells. The size and complexity of utrophin and dystrophin molecules limit biochemical and structural analysis of the full-length proteins. In contrast, analysis of individual domain constructs and, in particular, the respective N-terminal ABDs is more feasible and, in the current study, three distinct binding constructs were studied by EM and 3D reconstruction. Utr261 and Dys246 contained the ABD CH domains of the respective giant cytoskeletal proteins, and Utr416 included the first spectrin-repeat module of utrophin in addition to its CH domains. The biochemical characteristics of these and related constructs have been studied extensively elsewhere and again here.<sup>21,22,30,32–37</sup> Both negative staining and cryo-EM showed uniform decoration of F-actin by the utrophin constructs, conforming to the straightforward binding kinetics of monomeric utrophin to actin as a 1:1 complex.<sup>21</sup> We saw no compelling evidence of any heterogeneous labeling of F-actin by these constructs as reported in a recent study on F-actin–Utr261 by Galkin *et al.*<sup>27</sup> EM showed that Dys246 decorated F-actin uniformly without crosslinking the filaments.<sup>38</sup> Binding studies showed Dys246 associating with actin at a molar stoichiometry approaching 2:1 (Dys246:actin), and the molar excess protein bound was reflected by the slightly wider diameter of the Dys246 decorated filaments compared with the Utr261 labeled ones.

### Localization of utrophin on actin

The binding sites of utrophin on the periphery of F-actin were localized using EM and helical reconstruction of F-actin decorated with Utr261 and Utr416. Both constructs associated with the top of subdomain 1 of actin and projected azimuthally towards subdomains 3 and 4 over the trough formed by the shallow aspect of actin subdomain 2. This binding site was indistinguishable from those found previously for CH domains in reconstructions of  $\alpha$ -actinin, calponin, fimbrin and utrophin on F-actin.<sup>26–28,39,40</sup> The overall lozenge shape of utrophin CH domains, especially apparent in our 3D reconstructions of Utr261, was remarkably similar to that deduced for the pair of CH domains in fimbrin,<sup>28</sup> but differed from Utr261 densities first described by Moores *et al.*<sup>26</sup> and was larger than that illustrated recently by Galkin *et al.*<sup>27</sup> (discussed later).

Reconstructions of F-actin–Utr416 delineated the same CH domain densities as found in our Utr261 maps and revealed an extra mass that was connected to the inner tip of the CH domain moiety and lay longitudinally along the cleft between actin subdomains, i.e. near the junction of actin inner and outer domains where tropomyosin is located when on actin. The extra density was oriented roughly perpendicular to the CH domains and, no doubt, was contributed by the spectrin-repeat, which is not present in Utr261. Taken

together with binding measurements indicating a 1:1 stoichiometry of Utr416 and actin, these results suggested that the constituent CH and spectrin domains interact with F-actin as a unit and not independently. The binding of one end of the CH domain density on actin subdomain 1, while the other end is linked to spectrin defined the overall 50–60 Å length of CH1CH2 in both Utr261 and Utr416 ABDs. Since the spectrin-repeat module of utrophin is attached to the C-terminal end of CH2, CH2 would be expected to be close to spectrin on the inner domain of actin. Conversely, CH1 presumably resides more peripherally on actin.

Our helical reconstruction of F-actin decorated with the Utr261 ABD was particularly well defined and showed directly the outline of the entire molecular volume of the CH domain pair, which has not always been as obvious in other studies. This became especially evident after inspecting the crystal structure of Utr261 variously fitted into the corresponding Utr261 density envelopes of our reconstruction. As mentioned, the Utr261 density in our reconstructions mapped as a discrete mass with dimensions roughly 30 Å × 30 Å × 55–60 Å and showed no evidence of cross-connectivity to neighboring Utr261 molecules. The atomic structure of Utr261<sup>19</sup> modeled in a compact closed conformation like that of fimbrin<sup>20</sup> has similar dimensions and inserted very well into the EM density envelope of this structure.

In principle, fitting the atomic structure of asymmetrically shaped Utr416 into its corresponding EM envelope could have defined the relative positions of the CH1 and CH2 domains as well as the constituent spectrin-module on actin. However, no atomic structure of Utr416 is available and our own attempts at crystallizing Utr416 thus far have not succeeded, possibly because of the presence of a short flexible linker between CH domains and spectrin modules in the construct used, which is present in utrophin itself. We therefore attempted to determine the most plausible orientation for spectrin modules and CH domains by juxtaposing the known crystal structures of each fitted as separate rigid bodies to their respective EM envelopes. The only satisfactory arrangement was to orient CH domains in compact conformation with CH2 next to the inner domain of actin and CH1 positioned largely over the outer edge of actin subdomain 1, i.e. in the orientation that we suggested above. Indeed, this arrangement, depicted in Figure 6, is identical with that chosen for the docking of fimbrin's CH domains on F-actin, decided upon, in part, from biochemical inferences based on the binding of ABS-peptides and actin.<sup>29</sup> Conclusions drawn from the binding of short peptides have not always proven to be reliable, and we based our fitting here solely on geometrical parameters and inter-domain proximity. The consistency between the two analyses strengthens the conclusions of both. The overall similarity in molecular organization of CH domains in such functionally distinct proteins as fimbrin and

utrophin suggests that the binding interface and interactions of the CH domains are conserved.

Hydrodynamic data show that the CH1 and CH2 subdomains of Utr261 associate together as a compact monomer without any suggestion of an extended open arrangement.<sup>21</sup> In the current study, we found that this closed structure is maintained after binding of the ABD to F-actin. In contrast, in the crystal form of Utr261, an extended dumbbell-like structure is stabilized by dimerization.<sup>19</sup> This observation raised the possibility that such an elongated open conformation might be induced and stabilized by utrophin binding to F-actin.<sup>21</sup> Even though we saw no evidence of extended structures here, modeling of previously obtained reconstructions of Utr261 suggested this possibility, describing an  $\alpha$ -helical bridge that connected CH1 and CH2 subdomains on adjacent actin monomers along F-actin.<sup>26</sup> While we do not completely exclude the possibility of F-actin inducing an open conformation of Utr261, the alignment of data sets generating the earlier reconstruction and hence the component densities in the reconstruction were not reliable enough to have validated this hypothesis. By contrast, our new reconstructions of F-actin–Utr261, showing the ABD as a closed structure, were generated using stringent criteria to ensure proper alignment and filament polarities (see Materials and Methods). Recently, Galkin *et al.* analyzed negatively stained F-actin–Utr261 by single particle methods.<sup>27</sup> Their results resembled ours but the utrophin density in their reconstructions did not extend very far in the azimuthal direction over subdomain 2. They proposed an extended ABD although they did not detect a definitive density connecting CH subdomains on adjacent actin monomers. As mentioned, we saw no evidence of such a connecting density either, but, in all four of our reconstructions of uniformly labeled filaments, we did see density extending azimuthally, no doubt reflecting a compact ABD configuration on F-actin.

Our reconstructions provide empirical evidence that CH1 and CH2 subdomains of the utrophin ABD very likely retain a compact conformation when bound on F-actin. The energetics of CH domain associations supports this conclusion. Previous studies show that virtually all of the Utr261 in solution is in a compact conformation, demonstrating the very high intramolecular affinity of CH1 and CH2.<sup>21</sup> This is not surprising, since the compact conformation excludes solvent from hydrophobic patches on CH1 and CH2, and the helix that connects them together. In contrast to these strong intramolecular forces, the binding affinities of Utr261 (i.e. CH1CH2) and other CH-domain based ABDs for actin are relatively weak and variously reported to be in the  $K_d$  range of 1–40  $\mu\text{M}$ . Moreover, the affinity of the CH1 segment itself for actin is even lower, and CH2 constructs by themselves do not bind actin at all.<sup>10,19,32,33,41</sup> Thus, it seems improbable that actin

could induce and stabilize weak extended CH domain interactions in competition with the strong tendency for CH1 and CH2 subdomains to self-associate. Even under non-physiological acid conditions used to crystallize Utr261, soluble protein present was monomeric (C.A.M., unpublished results) suggesting that the CH1CH2 domains do not undergo opening and dimerization except under extreme conditions at high concentrations of protein, where a compact structure again is produced in the crystal, in this case by domain swapping between monomers within the dimer.

### Localization of dystrophin on actin

Dys246, like the utrophin constructs tested, localized on the periphery of F-actin, bound to subdomain 1 of actin and projected azimuthally towards subdomains 3 and 4 over actin subdomain 2. However, the size and shape of the Dys246 label differed qualitatively from CH domains associated with utrophin, fimbriin,  $\alpha$ -actinin and calponin,<sup>28,39,40</sup> forming a bilobed density. One of the density lobes was similar to CH domains of the others but the second observed at a slightly higher radius has not been seen before in reconstructions of CH domain-containing proteins. Since the binding stoichiometry of Dys246 and actin approached 2:1, and Dys246 itself is in a monomer–dimer equilibrium in solution, it is possible that the extra density lobe represented the second pair of CH domains seen in the crystal structure of the Dys246 dimer. Molecular fitting of the crystal structure of the Dys246 dimer to the reconstructions showed that a CH1CH2 pair in compact configuration fit into the inner density lobe very well, but the edges of the outer density lobe were not defined well enough to make fitting of a second ABD meaningful. If CH domains of dystrophin do dimerize *in vivo*, dystrophin might then make more extensive contact with F-actin than would monomeric utrophin, an arrangement well suited for its presumed function to dissipate mechanical stress to the extracellular matrix. The binding of dystrophin on actin, of course, could also involve interactions of its associated spectrin-repeat modules, which have not been evaluated here.<sup>37</sup>

### Conclusions

Even though CH domains are a conserved feature of a wide variety of actin-binding proteins, it is well recognized that their binding affinity for actin filaments ( $K_d$  1–40  $\mu\text{M}$ ) is considerably lower than that found for most other classes of actin-associated proteins ( $K_d$  0.1 nM–1  $\mu\text{M}$ ).<sup>42</sup> Strategies that, in effect, reduce the diffusional freedom of CH domains near actin, seem to have evolved to circumvent the low-affinity binding, thereby enhancing actin associations. Fimbrin, for example, is compartmentalized in microvilli at

relatively high concentration along with a second actin-crosslinking protein, villin.<sup>43,44</sup> The binding affinities of dystrophin and utrophin CH domains for actin are particularly weak but, as shown here, spectrin modules also target the parent proteins to actin, enhancing the binding probability of the CH domain ABD interactions. This synergism was confirmed by Ervasti and colleagues,<sup>37,45</sup> who studied the binding of various length N-terminal constructs derived from utrophin and dystrophin. Thus, a model is emerging in which spectrin-repeats, interacting over variable stretches of filaments, and CH domains, localized more discretely, both contribute to actin binding. The use of multiple, moderate-affinity binding interactions may provide a means to modulate actin association flexibly at the cortical cytoskeleton of muscle and other cells. Our studies have localized CH domains and spectrin-repeat modules on F-actin and represent an important step in understanding the overall architecture of utrophin and dystrophin links to the cytoskeleton. Comparison of the structural contribution of these two cytoskeletal proteins is essential for assessing the value of genetic replacement of dystrophin with utrophin in individuals suffering from Duchenne and Becker muscular dystrophy.

## Materials and Methods

### Protein expression

#### Expression and purification of utrophin 416 (Utr416)

The rat utrophin construct (for utrophin amino acid residues 2–416) was prepared by PCR from the UT11 plasmid<sup>30</sup> (residues 2–594) and was inserted as an *Xba*I/*Nco*I fragment into the pRSET-A vector (Invitrogen). *Escherichia coli* C41(DE3)<sup>46</sup> were transformed with this construct and grown in 2 × TY medium plus 0.1 mg/ml of ampicillin at 37 °C (to  $A_{600\text{ nm}}$  0.5–0.6) whereupon 0.2 mM isopropyl-β,D-thiogalactopyranoside (IPTG) was added to induce protein expression, and the cells grown overnight at 20 °C. The cells were harvested, washed in PBS and frozen in liquid N<sub>2</sub>. The cell pellet was thawed and resuspended in 200 mM NaCl, 3 mM β-mercaptoethanol, 10 mM imidazole (pH 7.4), 20 mM Tris buffer (pH 8.0) plus a Complete™ protease inhibitor cocktail tablet (Roche) and lysozyme (1 mg/ml), and then incubated on ice for 20 minutes. Cell lysis was completed by sonication for two 30 second bursts and the lysate centrifuged at 125,000g for one hour. The lysis supernatant was applied to Ni<sup>2+</sup>-NTA resin (Qiagen), equilibrated in 200 mM NaCl, 3 mM β-mercaptoethanol, 10 mM imidazole (pH 7.4), 20 mM Tris buffer (pH 8.0), washed extensively and the Utr416 eluted with 250 mM imidazole buffer (pH 7.4) as described in the manufacturer's manual. Fraction purity was confirmed by SDS-PAGE and protein concentrations were determined using the calculated extinction coefficient of 60,170 M<sup>-1</sup> cm<sup>-1</sup>. Utr416 was dialyzed against 200 mM NaCl, 1 mM DTT, 1 mM EGTA, 1 mM NaN<sub>3</sub>, 20 mM Tris buffer (pH 8.0) and concentrated with a Centriprep 30 (Millipore). Any aggregated material was removed by centrifugation at 174,000g for 15 minutes. The Utr416 was run on a calibrated Superdex 200 HR

30/10 gel-filtration column and it eluted as a single 52 kDa monomer peak. (The column was calibrated with five or six standards and Utr416 eluted between bovine serum albumin (67 kDa) and ovalbumin (43 kDa).)

The binding of Utr416 to F-actin was analyzed by a co-sedimentation assay, run under conditions identical with those described by Moores and Kendrick-Jones<sup>21</sup> in a solution of 100 mM NaCl, 2 mM MgCl<sub>2</sub>, 1 mM ATP, 1 mM DTT, 0.1 mM CaCl<sub>2</sub>, 20 mM Tris buffer (pH 8.0). The assay revealed that the Utr416 construct binds to F-actin with a stoichiometry of 1:1, the same ratio as that reported for Utr261<sup>21</sup> and confirmed here. Calibrated gel-filtration measurements indicated that both Utr416 and Utr261 were monomeric in solution. Thus, the presence of the spectrin-repeat on Utr416 did not affect the binding stoichiometry of the ABD or cause oligomerization.

#### Expression and purification of dystrophin 246 (Dys246)

The Dys246 (residues 1–246) construct<sup>18</sup> was cloned into the non-fusion pSJW1 vector<sup>21</sup> and expressed in *E. coli* C41(DE3) as described above, except that 0.5 mM IPTG was used for induction and the overnight incubation temperature was 25 °C. The two cysteine residues in this dystrophin construct at positions 10 and 188 had been mutated to serine, as described.<sup>18</sup> This modification was necessary to prevent the expressed protein from aggregating (a native conformation was especially important for measuring F-actin binding and carrying out meaningful structural work). The cell pellets expressing Dys246 were resuspended in 20 ml of 25% (w/v) sucrose, 1 mM EDTA, 1 mM DTT, 20 mM Tris buffer (pH 8.0), and a Complete™ protease inhibitor cocktail (Roche), and the cells were lysed by repeated freeze/thawing followed by four 30 second sonication bursts. The soluble Dys246 after centrifugation at 178,000g for 30 minutes was loaded onto a CM Sepharose Fastflow column (25 ml volume; washed and equilibrated in 1 mM EGTA, 1 mM NaN<sub>3</sub>, 1 mM DTT, 20 mM Tris buffer (pH 8.0)). The Dys246 was eluted with a linear gradient of NaCl from 0 mM to 200 mM in the same buffer. Fractions containing Dys246 were identified by SDS-PAGE, pooled and concentrated using an Amicon ultrafiltration cell under N<sub>2</sub> (Millipore). Any aggregated material was removed by centrifugation at 174,000g for 15 minutes. It was purified further by gel-filtration on a calibrated Superdex S200 column in 200 mM NaCl, 1 mM EGTA, 1 mM NaN<sub>3</sub>, 1 mM DTT, 20 mM Tris buffer (pH 8.0) and concentrated using a Centriprep 10 (Millipore). Following gel-filtration, purified Dys246 eluted as two peaks, corresponding to monomeric and dimeric species. Equilibrium sedimentation centrifugation confirmed that the two peaks were monomer and dimer, and that they existed in solution in a monomer–dimer equilibrium with a dissociation constant of  $6.3(\pm 0.2) \times 10^{-6}$  M. The binding of this expressed Dys246 to F-actin, measured by the co-sedimentation assay described above, approached a 2:1 molar ratio.

#### Expression and purification of utrophin 261 (Utr261)

Utr261 (residues 1–261) was expressed in *E. coli* and purified as described.<sup>21</sup>

## Electron microscopy and helical reconstruction

### Negative staining

F-actin (10  $\mu\text{M}$ ), prepared as described<sup>47</sup> was decorated with an excess of either Utr261 (100–150  $\mu\text{M}$ ), Utr416 (50  $\mu\text{M}$ ) or Dys246 (100–200  $\mu\text{M}$ ) in solutions consisting of 50 mM NaCl, 2 mM MgCl<sub>2</sub>, 1 mM EGTA, 1 mM NaN<sub>3</sub>, 10 mM Tris buffer, 5 mM sodium phosphate buffer at pH 7.1 and room temperature ( $\sim 25^\circ\text{C}$ ). Reconstituted filaments were diluted tenfold in the same buffer and were immediately applied to carbon-coated electron microscope grids, and negatively stained as described.<sup>48</sup> Grids were dried at 80% relative humidity to aid in spreading the stain. Grids were not glow-discharged before use,<sup>27</sup> which in our hands resulted in poor filament staining. Electron micrograph images of decorated filaments were recorded on a Philips CM120 electron microscope at 60,000 $\times$  magnification under low-dose conditions ( $\sim 12 \text{ e}^-/\text{\AA}$ ) at a defocus of 0.5  $\mu\text{m}$ .

### Cryo-electron microscopy

F-actin (5  $\mu\text{M}$ ) was decorated with Utr261 (50  $\mu\text{M}$ ) in the same solution as described above at pH 8.0 but without phosphate buffer present.<sup>26</sup> Cryo-EM of these filaments was carried out as described<sup>26</sup> but at a higher nominal defocus of 2.4  $\mu\text{m}$ . This yielded sufficient contrast to carry out image processing despite the high level of background interference from unbound Utr261. The resulting reduction in resolution to  $\sim 35 \text{ \AA}$  was acceptable, given the increased ability to accurately index layer-lines, align reconstructions to each other and judge filament polarities. We previously tried to achieve higher resolution by using lower defocus settings,<sup>26</sup> but this did not seem warranted in the current work.

### The 3D reconstruction

Micrographs were digitized using a Zeiss SCAI scanner at a pixel size corresponding to 0.7 nm in the filaments. Well-preserved regions of the filaments were selected and straightened as described.<sup>40,49</sup> Helical reconstruction was carried out by standard methods<sup>50</sup> as described.<sup>31,51</sup> Filament data sets were chosen for averaging on the basis of several factors, including up-down phase differences (a measurement of filament polarity) and the relative phase agreement between data sets (a measurement of the geometrical agreement among filaments). The measurement of actin polarity is not always definitive in filaments that are fully decorated with CH-domains, and any errors made in the determination of filament polarity would have corrupted the averaged data; e.g. averaging populations of filaments in which one-third were deliberately assigned the wrong polarity resulted in “CH-domain densities” with decreased azimuthal dimensions. In the current study, several additional criteria were used to judge the accuracy of the polarity assignment. The top and the bottom surface of filaments were analyzed separately by splitting data into “near” and “far” sides to make sure that the calculated polarities of each side matched.<sup>50</sup> When possible, separate reconstructions were made of several segments from the same filament (segments were between five and ten actin crossover repeats in length) to ensure that the polarities determined for the successive stretches were equivalent. In ambiguous cases, filaments were reprocessed or rejected. Finally, all

image processing was performed interactively, and each individual filament reconstruction was evaluated by direct inspection before adding its data to a growing average. If the polarity of a filament reconstruction or its alignment to the average was not obvious by eye, the filament data were not included in the final reconstruction. The statistical significance of densities in reconstructions was evaluated from the standard deviations associated with contributing points as described.<sup>52,53</sup>

## Docking of crystal structure models into EM density maps

### Fitting F-actin

F-actin coordinates<sup>54</sup> were modeled to the decorated F-actin and F-actin control reconstructions manually using the program O.<sup>55</sup>

### Fitting the utrophin ABD (Utr261)

Visual inspection of the density attributable to Utr261 (calculated from difference maps of F-actin–Utr261 and F-actin) made clear that Utr261 was compact in nature and not elongated (Figures 4 and 5). A search model was built for the compact structure using utrophin coordinates (PDB code 1qag)<sup>19</sup> for a domain-swapped ABD. The model comprised CH1 from chain A (residues 31–148) and CH2 from chain B (residues 153–256). All solvent atoms were removed. A rigid body search of three rotational and three positional parameters needed to dock the Utr261 ABD crystal structure into the difference map was conducted using COLORES from the SITUS (v2) suite of programs.<sup>56,57</sup> These programs ranked solutions according to the correlation coefficients between test models and the EM density envelopes. The Utr261 ABD search coordinates were filtered to a resolution of 25  $\text{\AA}$ , the same resolution as the F-actin–Utr261 reconstruction. The positional parameters were constrained to a search space of the lozenge-shaped difference peak and inspected using O.<sup>55</sup>

### Fitting the utrophin ABD and spectrin-repeat in Utr416

No crystal structure which could be used for molecular docking has been determined for Utr416. Since the relative orientations of the constituent ABD and spectrin-repeat modules were not known, the two domains were fitted independently into the Utr416 difference density calculated for F-actin–Utr416 and F-actin. The ABD was docked in the same orientation and position as those established for Utr261, and this, therefore, defined the density envelope that could be attributed to the spectrin-repeat. Even though crystal structures of utrophin (and dystrophin) spectrin-repeats are not available, sequence homology (SMART protein domain web tool<sup>58</sup>) indicates that the modules assume a three-helix bundle conformation comparable to that of the repeats of spectrin and  $\alpha$ -actinin.<sup>59–61</sup> We used coordinates of the second spectrin-repeat from  $\alpha$ -actinin (residues 391–513, PDB code 1quu)<sup>62</sup> as a search model, which was docked using SITUS into a difference map calculated by subtracting maps of F-actin–Utr261 from F-actin–Utr416. The fitting was conducted at a resolution of 32  $\text{\AA}$ , the same resolution as that calculated for the F-actin–Utr416 reconstruction.

### Fitting the dystrophin ABD (Dys246)

Visual inspection of the Dys246 difference map calculated from F-actin–Dys246 and F-actin revealed a predominantly compact mass similar to that of Utr261 but with an extra density lobe extending outward and down the filament (Figures 3 and 5). Initially, the fitting was conducted similarly to that of Utr261. A search model was built for a compact monomeric structure using a domain-swapped ABD from the dystrophin X-ray structure coordinates (PDB code 1dxx).<sup>18</sup> The model comprised CH1 from chain A (residues 9 to 130) and CH2 from chain B (residues 131 to 246). All solvent atoms were removed. SITUS was used to dock a dimeric dystrophin search template (chains A and B, residues 9–246) into the same difference density map using the full crystal structure of the dimer. Both docking runs were conducted at a resolution ~25 Å, the estimated resolution of the Dys246 reconstruction.

### Acknowledgements

We thank Dr Jo Butler for running the equilibrium sedimentation analysis on Dys246, and Drs Roberto Dominguez and Dorit Hanein for helpful discussion and useful criticism. The UT11 plasmid was kindly donated by Dr Marcus Schaub. These studies were supported by the Muscular Dystrophy Campaign of Great Britain and Northern Ireland (to A.J.S.-S. and J.K.-J.) and by the National Institutes of Health grants HL36153 (to W.L.), AR34711, HL62468 (to R.C.) and a Shared Instrument Grant, RR08426, for the purchase and maintenance of the CM120 electron microscope.

### References

- Gillis, J.-M. (2000). An attempt of gene therapy in Duchenne muscular dystrophy: overexpression of utrophin in transgenic *mdx* mice. *Acta Neurol. Belg.* **100**, 146–200.
- Keep, N. H. (2000). Structural comparison of actin binding in utrophin and dystrophin. *Neurol. Sci.* **21**, S929–S937.
- Blake, D. J., Weir, A., Newey, S. E. & Davies, K. E. (2002). Function and genetics of dystrophin and dystrophin-related proteins in muscle. *Physiol. Rev.* **82**, 291–329.
- Winder, S. J., Knight, A. E. & Kendrick-Jones, J. (1997). Protein structure. In *Dystrophin, Gene, Protein and Cell Biology* (Brown, S. C. & Lucy, J. A., eds), pp. 27–55, Cambridge University Press, Cambridge, UK.
- Ervasti, J. M. & Campbell, K. P. (1993). A role for the dystrophin–glycoprotein complex as a transmembrane linker between laminin and actin. *J. Cell Biol.* **122**, 809–823.
- Pascual, J., Castresana, J. & Saraste, M. (1997). Evolution of the spectrin repeat. *Bioessays*, **19**, 811–817.
- Castresana, J. & Saraste, M. (1995). Does Vav bind to F-actin through a CH domain? *FEBS Letters*, **374**, 149–151.
- Stradal, T., Kranewitter, W., Winder, S. J. & Gimona, M. (1998). CH domains revisited. *FEBS Letters*, **431**, 134–137.
- de Arruda, M. V., Watson, S., Lin, C. S., Leavitt, J. & Matsudaira, P. (1990). Fimbrin is a homologue of the cytoplasmic phosphoprotein plastin and has domains homologous with calmodulin and actin gelation proteins. *J. Cell Biol.* **111**, 1069–1079.
- Gimona, M., Djinovic-Carugo, K., Kranewitter, W. J. & Winder, S. J. (2002). Functional plasticity of CH domains. *FEBS Letters*, **513**, 98–106.
- Corrado, K., Mills, P. L. & Chamberlain, J. S. (1994). Deletion analysis of the dystrophin–actin binding domain. *FEBS Letters*, **344**, 255–260.
- Fabbrizio, E., Bonet-Kerrache, A., Leger, J. J. & Mornet, D. (1993). Actin–dystrophin interface. *Biochemistry*, **32**, 10457–10463.
- Kuhlman, P. A., Hemmings, L. & Critchley, D. R. (1992). The identification and characterisation of an actin-binding site in α-actinin by mutagenesis. *FEBS Letters*, **304**, 201–206.
- Hemmings, L., Kuhlman, P. A. & Critchley, D. R. (1992). Analysis of the actin-binding domain of α-actinin by mutagenesis and demonstration that dystrophin contains a functionally homologous domain. *J. Cell Biol.* **116**, 1369–1380.
- Bresnick, A. R., Warren, V. & Condeelis, J. (1990). Identification of a short sequence essential for actin-binding by Dictyostelium ABP-120. *J. Biol. Chem.* **265**, 9236–9240.
- Levine, B. A., Moir, A. J. G., Patchell, V. B. & Perry, S. V. (1992). Binding sites involved in the interaction of actin with the N-terminal region of dystrophin. *FEBS Letters*, **298**, 44–48.
- Morris, G. E., Man, N. T., Huyen, N. T. N., Pereboev, A., Kendrick-Jones, J. & Winder, S. J. (1999). Disruption of the utrophin–actin interaction by monoclonal antibodies and prediction of an actin-binding surface of utrophin. *Biochem. J.* **337**, 119–123.
- Norwood, F. L. M., Sutherland-Smith, A. J., Keep, N. H. & Kendrick-Jones, J. (2000). The structure of the N-terminal actin-binding domain of human dystrophin and how mutations in this domain may cause Duchenne or Becker muscular dystrophy. *Structure*, **8**, 481–491.
- Keep, N. H., Winder, S. J., Moores, C. A., Walke, S., Norwood, F. L. M. & Kendrick-Jones, J. (1999). Crystal structure of the actin-binding region of utrophin reveals a head-to-tail dimer. *Structure*, **7**, 1539–1546.
- Goldsmith, S. C., Pokala, N., Shen, W., Fedorov, A. A., Matsudaira, P. & Almo, S. C. (1997). The structure of an actin-crosslinking domain from human fimbriin. *Nature Struct. Biol.* **4**, 708–712.
- Moores, C. A. & Kendrick-Jones, J. (2000). Biochemical characterisation of the actin-binding properties of utrophin. *J. Cell Motil. Cytoskeleton*, **46**, 116–128.
- Norwood, F. L. M. (1999). Biochemical and structural studies on the actin binding N-terminal region of the dystrophin protein. PhD Thesis, University of London.
- Djinovic-Carugo, K., Gautel, M., Ylanne, J. & Young, P. (2002). The spectrin repeat: a structural platform for cytoskeletal protein assemblies. *FEBS Letters*, **513**, 119–123.
- Tinsley, J. M., Potter, A. C., Phelps, S. R., Fisher, R., Trickett, J. I. & Davies, K. E. (1996). Amelioration of the dystrophic phenotype of *mdx* mice using a truncated utrophin transgene. *Nature*, **384**, 349–353.
- Tinsley, J. M., Deconinck, N., Fisher, R., Kahn, D., Phelps, S., Gillis, J.-M. & Davies, K. E. (1998). Expression of full-length utrophin prevents muscular dystrophy in *mdx* mice. *Nature Med.* **12**, 1441–1444.

26. Moores, C. A., Keep, N. H. & Kendrick-Jones, J. (2000). Structure of the utrophin actin-binding domain bound to F-actin reveals binding by an induced fit mechanism. *J. Mol. Biol.* **297**, 465–480.
27. Galkin, V. E., Orlova, A., VanLoock, M. S., Rybakova, I. N., Ervasti, J. M. & Egelman, E. H. (2002). The utrophin actin-binding domain binds F-actin in two different modes: implications for the spectrin superfamily of proteins. *J. Cell. Biol.* **157**, 243–251.
28. Hanein, D., Matsudaira, P. & DeRosier, D. J. (1997). Evidence for a conformational change in actin induced by fimbrin (N375) binding. *J. Cell. Biol.* **139**, 387–396.
29. Hanein, D., Volkmann, N., Goldsmith, S., Michon, A. M., Lehman, W., Craig, R. et al. (1998). An atomic model of fimbrin binding to F-actin and its implications for filament crosslinking and regulation. *Nature Struct. Biol.* **5**, 787–792.
30. Zuellig, R. A., Bornhauser, B. C., Knuesel, I., Heller, F., Fritschy, J.-M. & Schaub, M. C. (2000). Identification and characterisation of transcript and protein of a new short N-terminal utrophin isoform. *J. Cell. Biochem.* **77**, 418–431.
31. Lehman, W., Hatch, V., Korman, V., Rosol, M., Thomas, L., Maytum, R. et al. (2000). Tropomyosin and actin isoforms modulate the localization of tropomyosin strands on actin filaments. *J. Mol. Biol.* **302**, 593–606.
32. Way, M., Pope, B., Cross, R. A., Kendrick-Jones, J. & Weeds, A. G. (1992). Expression of the N-terminal domain of dystrophin in *E. coli* and demonstration of binding to F-actin. *FEBS Letters*, **301**, 243–245.
33. Winder, S. J., Hemmings, L., Maciver, S. K., Bolton, S. J., Tinsley, J. M., Davies, K. E. et al. (1995). Utrophin actin binding domain: analysis of actin binding and cellular targeting. *J. Cell. Sci.* **108**, 63–71.
34. Winder, S. J. (1996). Structure–function relationships in dystrophin and utrophin. *Biochem. Soc. Trans.* **24**, 497–501.
35. Amann, K. J., Renley, B. A. & Ervasti, J. M. (1998). A cluster of basic repeats in the dystrophin rod domain binds F-actin through an electrostatic interaction. *J. Biol. Chem.* **273**, 28419–28423.
36. Renley, B. A., Rybakova, I. N., Amann, K. J. & Ervasti, J. M. (1998). Dystrophin binding to non-muscle actin. *Cell Motil. Cytoskeleton*, **41**, 264–270.
37. Rybakova, I. N., Patel, J. R., Davies, K. E., Yurchenco, P. D. & Ervasti, J. M. (2002). Utrophin binds laterally along actin filaments and can couple costameric actin with sarcolemma when overexpressed in dystrophin-deficient muscle. *Mol. Biol. Cell*, **13**, 1512–1521.
38. Orlova, A., Rybakova, I. N., Prochniewicz, E., Thomas, D. D., Ervasti, J. M., & Egelman, E. H. (2001). Binding of dystrophin's tandem calponin homology domain to F-actin is modulated by actin's structure. *Biophys. J.* **80**, 1926–1931.
39. McGough, A., Way, M. & DeRosier, D. (1994). Determination of the  $\alpha$ -actinin binding site on actin filaments by cryoelectron microscopy and image analysis. *J. Cell Biol.* **126**, 433–443.
40. Hodgkinson, J. L., El-Mezgueldi, M., Craig, R., Vibert, P., Marston, S. B. & Lehman, W. (1997). 3-D image reconstruction of reconstituted smooth muscle thin filaments containing calponin: visualization of interactions between F-actin and calponin. *J. Mol. Biol.* **273**, 150–159.
41. Djinovic-Carugo, K., Banuelos, S. & Saraste, M. (1997). Crystal structure of a calponin homology domain. *Nature Struct. Biol.* **4**, 175–179.
42. Pollard, T. D. & Earnshaw, W. C. (2002). Actin and actin binding proteins. In *Cell Biology*, Chapt. 36, Saunders, Philadelphia pp. 566–567.
43. Heintzelman, M. B. & Mooseker, M. S. (1992). Assembly of the intestinal brush border cytoskeleton. *Curr. Top. Dev. Biol.* **26**, 93–122.
44. Louvard, D., Kedinger, M. & Hauri, H. P. (1992). The differentiating intestinal epithelial cell: establishment and maintenance of functions through interactions between cellular structures. *Annu. Rev. Cell Biol.* **8**, 157–195.
45. Amann, K. J., Renley, B. A. & Ervasti, J. M. (1998). A cluster of basic repeats in the dystrophin rod domain binds F-actin through an electrostatic interaction. *J. Biol. Chem.* **273**, 28419–28423.
46. Miroux, B. & Walker, J. E. (1996). Over-production of proteins in *Escherichia coli*: mutant hosts that allow synthesis of some membrane proteins and globular proteins at high levels. *J. Mol. Biol.* **260**, 289–298.
47. Spudich, J. A. & Watt, S. (1971). The regulation of rabbit skeletal muscle contraction. I. Biochemical studies of the interaction of the tropomyosin–tropo-nin complex with actin and the proteolytic fragments of myosin. *J. Biol. Chem.* **246**, 4866–4871.
48. Moody, C., Lehman, W. & Craig, R. (1990). Caldesmon and the structure of vertebrate smooth muscle thin filaments: electron microscopy of isolated thin filaments. *J. Muscle Res. Cell Motil.* **11**, 176–185.
49. Egelman, E. H. (1986). An algorithm for straightening images of curved filamentous structures. *Ultramicroscopy*, **19**, 367–374.
50. Owen, C., Morgan, D. G. & DeRosier, D. J. (1996). Image analysis of helical objects: the Brandeis helical package. *J. Struct. Biol.* **116**, 167–175.
51. Vibert, P., Craig, R. & Lehman, W. (1993). Three-dimensional reconstruction of caldesmon-containing smooth muscle thin filaments. *J. Cell Biol.* **123**, 313–321.
52. Milligan, R. A. & Flicker, P. F. (1987). Structural relationships of actin, myosin and tropomyosin revealed by cryo-electron microscopy. *J. Cell Biol.* **105**, 29–39.
53. Trachtenberg, S. & DeRosier, D. J. (1987). Three-dimensional structure of frozen hydrated flagellar filament of *Salmonella typhimurium*. *J. Mol. Biol.* **195**, 581–601.
54. Lorenz, M., Popp, D. & Holmes, K. C. (1993). Refinement of the F-actin model against X-ray fiber diffraction data by use of a directed mutation algorithm. *J. Mol. Biol.* **234**, 826–836.
55. Jones, T. A., Zou, J. Y., Cowan, S. W. & Kjeldgaard, M. (1991). Improved methods for the building of protein models in electron density maps and the location of errors in these models. *Acta Crystallogr. sect. A*, **47**, 110–119.
56. Wriggers, W., Milligan, R. A. & McCammon, J. A. (1999). Situs: a package for docking crystal structures into low-resolution maps from electron microscopy. *J. Struct. Biol.* **125**, 185–195.
57. Chacon, P. & Wriggers, W. (2002). Multi-resolution contour-based fitting of macromolecular structures. *J. Mol. Biol.* **317**, 375–384.
58. Schultz, J., Copley, R. R., Doerk, T., Ponting, C. P. & Bork, P. (2000). SMART: a web-based tool for the study of genetically mobile domains. *Nucleic Acids Res.* **28**, 231–234.

59. Yan, Y., Winograd, E., Viel, A., Cronin, T., Harrison, S. C. & Branton, D. (1993). Crystal structure of the repetitive segments of spectrin. *Science*, **262**, 2027–2030.
60. Pascual, J., Castresana, J. & Saraste, M. (1997). Evolution of the spectrin repeat. *Bioessays*, **19**, 811–817.
61. Grum, V. L., Li, D., MacDonald, R. I. & Mondragon, A. (1999). Structures of two repeats of spectrin suggest models of flexibility. *Cell*, **98**, 523–535.
62. Djinovic-Carugo, K., Young, P., Gautel, M. & Saraste, M. (1999). Structure of the alpha-actinin rod: molecular basis for cross-linking of actin filaments. *Cell*, **98**, 537–546.
63. Humphrey, W., Dalke, A. & Shulten, K. (1996). VMD: visual molecular dynamics. *J. Mol. Graph.* **14**, 33–38.

*Edited by W. Baumeister*

(Received 17 January 2003; received in revised form 24 March 2003; accepted 24 March 2003)